Structural, transport, and magnetic properties of narrow bandwidth $Nd_{1-x}Ca_xCoO_{3-\delta}$ and comparisons to $Pr_{1-x}Ca_xCoO_{3-\delta}$

D. Phelan,[1] Y. Suzuki,[1] S. Wang,[1] A. Huq,[2] and C. Leighton[1]

[1]*Department of Chemical Engineering and Materials Science, University of Minnesota, Minneapolis, Minnesota 55455, USA*

[2]*Chemical and Engineering Materials Division, Oak Ridge National Laboratory, Oak Ridge, Tennessee 37831, USA*

(Received 22 May 2013; published 9 August 2013)

Low bandwidth Pr-based cobalt perovskites, such as $Pr_{1-x}Ca_xCoO_{3-\delta}$, have received significant recent attention as they undergo first-order spin-state transitions with a strong influence on magnetic and transport properties. The unique nature of the Pr-O bond has been implicated as the impetus for these transitions, as it is thought that temperature-dependent charge transfer can occur between Pr and Co ions, i.e., a partial $Pr^{3+} \rightarrow Pr^{4+}$ and $Co^{4+} \rightarrow Co^{3+}$ valence shift. In the present work, we have studied the related compound $Nd_{1-x}Ca_xCoO_{3-\delta}$. The Nd^{3+} ions have very similar ionic radius to Pr^{3+} but do not induce a temperature-dependent valence shift (at least in the composition range studied here), enabling deconvolution of the intrinsic low bandwidth physics from the unique effects of Pr-O bonding in $Pr_{1-x}Ca_xCoO_{3-\delta}$. To this end, we have characterized the structural, magnetic, and electronic transport characteristics of $Nd_{1-x}Ca_xCoO_{3-\delta}$ bulk polycrystals, using neutron diffraction, small-angle neutron scattering, dc and ac magnetometry, and magnetotransport, and have established the $Nd_{1-x}Ca_xCoO_{3-\delta}$ magnetic phase diagram. This phase diagram contains regimes of short-range ferromagnetism and long-range ferromagnetism, in addition to ferrimagnetism. We argue that, with the exception of the valence transition that occurs at high x (e.g., $x = 0.5$) in $Pr_{1-x}Ca_xCoO_{3-\delta}$ and the low-temperature ordering of Nd^{3+}moments that results in the ferrimagnetism in $Nd_{1-x}Ca_xCoO_{3-\delta}$, the two systems are nearly isostructural and have similar magnetic and transport properties. The low bandwidth physics intrinsic to both systems is summarized as encompassing long-range ferromagnetism with a relatively low Curie temperature due to Co-O-Co bond buckling (<60 K for $Nd_{1-x}Ca_xCoO_{3-\delta}$), short-range ferromagnetism that emerges at much higher temperatures (~270 K for $Nd_{1-x}Ca_xCoO_{3-\delta}$), and likely stems from oxygen deficiency, exchange-spring behavior related to magnetoelectronic phase separation, and a doping-driven insulator-metal transition. In addition to elucidating the essential physics of narrow bandwidth perovskite cobaltites, the results thus further confirm the importance of the unique features of the Pr-O bond in driving the abrupt spin-state transition in $Pr_{1-x}Ca_xCoO_{3-\delta}$.

DOI: 10.1103/PhysRevB.88.075119 PACS number(s): 61.05.fg, 61.05.fm, 72.80.Ga, 75.47.Gk

I. INTRODUCTION

Perovskite cobaltites (with chemical formula $RCoO_3$) exhibit a plethora of intriguing physical phenomena, including spin-state crossovers, transitions from insulating to metallic transport, and magnetoelectronic phase separation. A well-studied representative of the varied behaviors of these compounds is provided by $La_{1-x}Sr_xCoO_3$ (LSCO). Its parent compound, $LaCoO_3$ ($x = 0$) undergoes a gradual thermally driven spin-state crossover from a nonmagnetic ground state (Co^{3+} in the $t_{2g}^6e_g^0$, $S = 0$ configuration) to a paramagnetic state (Co^{3+} in the $t_{2g}^5e_g^1$, $S = 1$ or $t_{2g}^4e_g^2$, $S = 2$ configuration) with a "spin gap" of only 10 to 20 meV.[1] The exact nature of this transition remains controversial, particularly the issue of $S = 1$ vs $S = 2$ (or some mixture), despite more than half a century of research.[1–4] As holes are chemically introduced through the substitution of Sr^{2+} for La^{3+}, seven-site magnetopolarons (also referred to as spin-state polarons) appear at low x,[5,6] followed by a regime of magnetoelectronic phase separation from $x = 0.04$ to 0.22. The percolation of ferromagnetic clusters induces an insulator-metal transition (IMT) at $x = 0.17$–0.18,[7] coincident with the emergence of long-range ferromagnetic order. The regime prior to percolation is characterized as having ferromagnetic clusters embedded in a nonferromagnetic matrix,[8] with phase competition between the percolated network and incommensurate spin correlations being observed by neutron diffraction.[9] Above $x = 0.22$, a uniform ferromagnetic metallic phase is found, with a Curie temperature (T_C) that reaches 250 K at $x = 0.5$. Recently, it has been pointed out that many features of the phase separation in the regime $0.04 < x < 0.22$ can be understood within a simple statistical model, focusing on the inevitable nanoscale variations in local doping concentration.[7]

In terms of structure, LSCO is a rhombohedrally distorted perovskite (space group $R\bar{3}c$), with antiphase rotations of the $CoO_{6/2}$ octahedra ($\mathbf{a^-a^-a^-}$ in the Glazer tilt system[10]), leading to only slightly obtuse Co-O-Co angles.[11] If, instead of La, a smaller ion is substituted at the A site, such as Pr or Nd, the structure tends to adopt orthorhombic symmetry (space group $Pnma$, $\mathbf{a^-b^+a^-}$ in Glazer notation), yielding significantly smaller Co-O-Co bond angles.[12–14] This distortion has important consequences for the magnetic and electronic properties. First, it increases the energy gap between the Co^{3+} $S = 0$ state and the excited magnetic Co^{3+} states, as evidenced by an increase in the onset temperatures for the spin-state transition in $NdCoO_3$ and $PrCoO_3$ compared to $LaCoO_3$.[15,16] Second, in hole-doped compounds, where ferromagnetic interactions and charge transport are commonly understood to arise from double exchange, buckling of the Co-O-Co bonds leads to reduced ferromagnetic exchange interactions and lower electronic bandwidth. These two factors are expected to result in important new physics due to both the enhancement of magnetoelectronic phase separation (from the suppression of dominant metallic ferromagnetism compared to

other phases) and the anticipated stronger interplay between phase separation and spin-state physics.[17] Low bandwidth cobaltites are thus of significant interest.

Recently, $Pr_{1-x}Ca_xCoO_{3-\delta}$ (PCCO) has been thoroughly investigated as a prototype low bandwidth cobaltite. Suppressed long-range ferromagnetism and enhanced magneto-electronic phase separation have indeed been observed, along with an unanticipated exchange-spring-type behavior due to coupling between long- and short-range ordered magnetic regions.[18] Moreover, an intriguing first-order IMT has been reported for $Pr_{0.5}Ca_{0.5}CoO_3$ (Ref. 19; at $T_{MI} \sim 100$ K) and $(Pr_{1-z}Y_z)_{0.7}Ca_{0.3}CoO_3$,[20] and accounted for, quite remarkably, by an abrupt transfer of electrons from Pr to Co,[21,22] i.e., a temperature-dependent change in Pr valence. This is accompanied by a large reduction in Co magnetic moment on cooling, attributed to an abrupt spin-state transition.[19] Importantly, density functional theory calculations indicate that the Pr $4f$ states lie only ~0.5 eV below the Fermi level above T_{MI}, but become gapped below T_{MI}, with some of the states pushed above the Fermi level. Electrons are transferred from the Pr $4f$ orbitals to the Co $3d$ states, which are hybridized with O $2p$ states.[21] For $Pr_{0.5}Ca_{0.5}CoO_3$, on the basis of x-ray absorption spectroscopy, it has been estimated that the average valences of Pr and Co are described by the following transformation on cooling: $\frac{1}{2}\,Pr^{3+} + Co^{3.5+} \rightarrow \frac{1}{2}\,Pr^{3.52+} + Co^{3.24+}$.[23] Furthermore, in the Sr-doped analog, $Pr_{1-x}Sr_xCoO_3$, it is notable that a coupled structural/magnetic anisotropy transition had been previously observed for $x = 0.5$ and again accounted for by Pr-O hybridization.[24] Unusual features of Pr-O bonding have also been implicated in the unique behavior in other oxides, such as the anomalous insulating behavior found in $PrBa_2Cu_3O_{7-y}$.[25] While Pr-based cobaltites thus contain a wealth of interesting physics, many of these properties may well result from the specific role of the unique Pr-O bond. One may therefore wonder about the physics of low bandwidth cobaltites in the absence of Pr, which motivated us to carry out a thorough investigation of $Nd_{1-x}Ca_xCoO_{3-\delta}$ (NCCO). Since Nd^{3+} has a similar ionic radius to that of Pr^{3+} (it is ~1.6% smaller[26]) but is not anticipated to hybridize with oxygen (computational work suggests that Nd $4f$ electrons in NCCO lie too far below the Fermi level to permit Nd-O covalency effects[21]), we argue that it can serve as a control system to deconvolute the intrinsic narrow bandwidth physics from the Pr-O bonding effects in PCCO.

In this work, we have used neutron diffraction to determine the structural parameters, dc and ac magnetometry, neutron diffraction, and small-angle neutron scattering (SANS) to investigate magnetic properties, and temperature- and field-dependent resistivity measurements to assess the magneto-transport properties of NCCO. We show, at least for $x \leqslant 0.3$, that NCCO and PCCO adopt very similar structures. We find that NCCO becomes long-range ordered ferromagnetic (LROFM) for $x \geqslant 0.075$ (with a slightly reduced T_C compared to PCCO) and that the Nd^{3+} moments order antiparallel to the Co moments below $T_{\text{Ferri}} \sim 0.25\ T_C$. Evidence for a relatively hard, short-range ordered ferromagnetic (SROFM) phase is also seen below ~270 K, likely related to oxygen deficiency. This leads to exchange-spring behavior at the SROFM/LROFM interface, as in PCCO. Transport measurements provide evidence of a zero temperature IMT around $x = 0.10$ to 0.15, with typical negative magnetoresistance (MR) effects around T_C of about 3% in the high x metallic phase. A magnetic and electronic phase diagram is thus established for NCCO, enabling us to conclude that the main differences between NCCO and PCCO are the low-temperature Nd^{3+} magnetic ordering in NCCO and the valence transition that occurs at large x in PCCO. The Nd valence transition was, in fact, not observed over the entire composition range studied in NCCO ($0 \leqslant x \leqslant 0.4$). Otherwise, both systems exhibit magnetic phase separation, low-temperature LROFM (with volume fractions well below unity), higher-temperature oxygen-deficiency-related SROFM, exchange spring effects due to coupling between SROFM and LROFM regions, and metallic ground states at high x.

II. EXPERIMENTAL DETAILS

Polycrystalline samples of NCCO were synthesized by solid-state reaction from the starting compounds Co_3O_4, $CaCO_3$, and Nd_2O_3. These reactants were ground together and reacted at 1000 °C for 24 h in air. The resulting powder was reground, and (with the exception of the samples measured using neutron diffraction) pressed into a cylindrical pellet. Due to the required mass of powder samples for neutron diffraction, they were not pressed into pellets in an effort to better oxygenate the entire samples. The pellets (or powders) were then subsequently annealed at 1100–1200 °C in flowing O_2 for 24 h and then cooled to room temperature at a rate of 0.5 °C/min. The phase purity of all samples was checked by laboratory (Cu-$K\alpha$) x-ray diffraction. As x was increased, a minority impurity phase, which we were unable to identify, was observed to appear. Slow cooling in oxygen during the last step of the synthesis was sufficient to limit the quantity of this phase for $x \leqslant 0.4$; however, the impurity phase became more substantial for $x > 0.4$, and thus we limited our studies to $x \leqslant 0.4$.

Powder neutron diffraction measurements were performed on the time-of-flight diffractometer, POWGEN, located at the Spallation Neutron Source at Oak Ridge National Laboratory. Measurements were made with central wavelengths of 1.066 and 3.731 Å, covering a d-spacing range of 0.3 to 8.2 Å. The samples were sealed in cylindrical vanadium containers under a helium atmosphere and were measured in a closed-cycle refrigerator (CCR) between 8 and 300 K. Refinement was carried out using the General Structure Analysis System (GSAS; Ref. 27) with the EXPGUI graphical user interface.[28] SANS measurements were performed on pressed pellets of an $x = 0.4$ sample on the NG-3 beamline at the National Institute of Standards and Technology Center for Neutron Research[29,30] at a wavelength of 6 Å. The sample was measured in a CCR at temperatures between 4 and 300 K. The dc and ac magnetometry was performed on small pieces of sintered pellets in a Quantum Design Magnetic Property Measurement System (MPMS) superconducting quantum interference device (SQUID) magnetometer or a Quantum Design Physical Property Measurement System (PPMS) vibrating sample magnetometer from temperatures of 2 to 300 K and in applied magnetic fields up to $\mu_o H = 7$ T. Transport measurements were performed by conventional dc and ac (13.7 or 16 Hz) methods using a standard van der Pauw technique with the

sample in a helium atmosphere from temperatures of 4.2 to 300 K and magnetic fields up to $\mu_o H = 9$ T. Contacts were made by directly soldering In or by sputtering a 50-Å-thick layer of Mg, followed by a 500-Å layer of Au, and then soldering on top of the Au layer with In. Care was taken to check for ohmic response at low temperatures.

III. RESULTS AND ANALYSIS

A. Crystal structure

The crystal structure of PCCO has been thoroughly investigated. It was found to have orthorhombic symmetry for $0 \leqslant x \leqslant 0.5$ (space group *Pnma*, or alternatively *Pbnm*), commonly adopted in perovskites,[12–14,31,32] and often observed when the tolerance factor, $t = (r_A + r_O)/[\sqrt{2}(r_B + r_O)]$, where r_A, r_B, and r_O are the ionic radii of the A site, B site, and O ions, lies 0.75 and 0.9.[33] The defining characteristic of this structure is the oxygen octahedral rotation pattern ($\mathbf{a^-b^+a^-}$). The similar sizes of Nd^{3+} and Pr^{3+} ions suggest that NCCO and PCCO should likely have similar crystal structures. Indeed, room-temperature x-ray diffraction indicates the same orthorhombic symmetry for NCCO,[34] although to our knowledge a detailed structural refinement has thus far only been reported for the parent compound, $x = 0$.[13] Our own neutron diffraction measurements suggest that indeed the crystal structure of NCCO is orthorhombic for $0 \leqslant x \leqslant 0.4$ from 9 to 300 K (the entire composition and temperature range studied). Figure 1 shows a representative Rietveld refinement on an $x = 0.2$ sample at 300 K. The data and fits are shown both at a central wavelength of 1.066 Å [Fig. 1(a)] and at 3.631 Å [Fig. 1(b)]. As mentioned in Sec. II, while the overall agreement is good, we observe some weak reflections [labeled with asterisks in Fig. 1(b)] that are not indexed within the *Pnma* space group. Several of these reflections appear as shoulders in the higher resolution ($\lambda = 3.631$ Å) data, decreasing the quality of the fit. These reflections grow stronger as x is increased. While the origin of these reflections is unclear, and we treat them here as an impurity phase as a first approximation, the fact that they increase with x suggests that they could be related to an oxygen-deficient phase. Oxygen vacancy ordering, which occurs in a number of perovskites (e.g., high x LSCO[35]) is a possibility that should not be discounted. The lattice constants and atom positions determined from the refinements are provided in Table I. Also listed is the refined oxygen occupancy, which decreases with increasing x, as expected from the general trends seen in other perovskite cobaltites. This is largely attributable to the Co^{3+} oxidation state being generally favored over Co^{4+} in this coordination.

The x dependence of the unit cell volume (V) of NCCO is compared to PCCO in Fig. 2(a) at low (∼10 K) and high (∼300 K) temperatures. For $x \leqslant 0.3$, the unit cell volumes of the NCCO samples are slightly smaller than their PCCO counterparts, stemming from the Nd^{3+} radius being ∼1.6% smaller than that of Pr^{3+}. Notably, there is little x dependence of the unit cell volume for NCCO at ∼300 K, and a weak decrease in unit cell volume is observed at ∼10 K as x is increased. This is somewhat surprising because the ionic radius of Ca is 5.5% larger than Nd in a 12-fold coordination.[36]

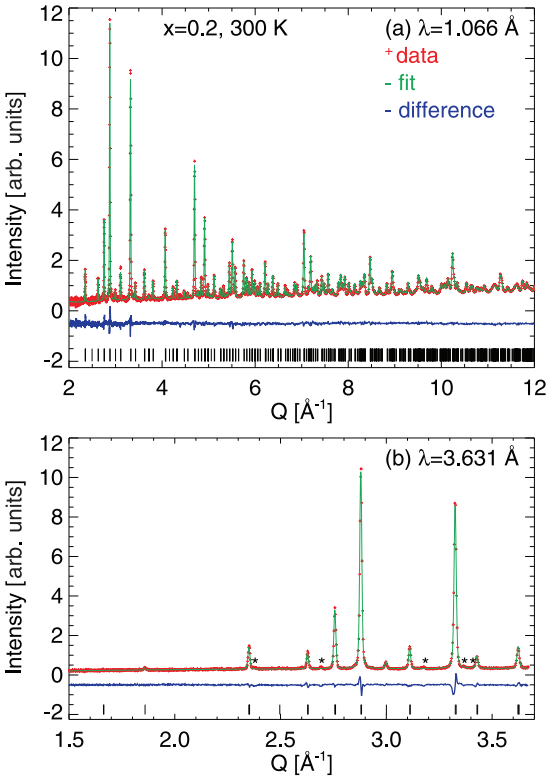

FIG. 1. (Color online) Rietveld refinement of $Nd_{0.8}Ca_{0.2}CoO_{3-\delta}$ at 300 K. The data are shown as red "+" symbols, the fit is shown as the continuous green curve, the difference plot is shown below the data as a continuous blue curve, and the allowed reflections for the *Pnma* space group are indicated by black tick marks. Data taken with a central wavelength of 1.066 Å are shown in (a), while data taken with a central wavelength of 3.631 Å are shown in (b). The positions of some weak reflections that are not described by this structural model are marked with an asterisk in (b).

Indeed, Ca is also larger than Pr, yet PCCO shows a similar decrease in cell volume with x for $x \leqslant 0.3$ (see also Ref. 31). At present, this is not understood. However, the unit cell volume is not only related to the A-site radii but is also influenced by changes in the average Co radius upon doping. While the Co^{4+} radius is smaller than Co^{3+}, the intermediate-spin or high-spin states of Co^{3+} are also larger than low-spin Co^{3+}. Moreover, the progression of the unit cell volume is also complicated by the cooperative rotations of the oxygen octahedra. The precipitous drop in unit cell volume from $x = 0.3$ to $x = 0.5$, the most striking feature of Fig. 2(a), is seen to be unique to PCCO, resulting from the metal-insulator and spin-state transitions that occur at $x = 0.5$, attributed to a change in the Pr valence.

The Co-O-Co bond angles are of significant importance as the overlap of the Co $3d$ and O $2p$ orbitals directly regulates the e_g bandwidth.[37] This, in turn, affects the strength of the exchange interaction between Co spins, as well as T_C. Figures 2(b) and 2(c) compare the Co-O-Co bond angles as a function of x at ∼10 and ∼300 K. (Note that there are two distinct Co-O-Co bond angles in the orthorhombic structure.) Both PCCO and NCCO have bond angles that are significantly distorted compared to an ideal cubic perovskite. The NCCO bond angles are smaller than the corresponding PCCO bond

TABLE I. Refined structural parameters for NCCO at 9 and 300 K in the *Pnma* space group. The Nd/Ca coordinates are (x_{Nd}, $\frac{1}{4}$, z_{Nd}); the Co coordinates are (0, 0, $\frac{1}{2}$); the O1 coordinates are (x_{O1}, $\frac{1}{4}$, z_{O1}); and the O2 coordinates are (x_{O2}, y_{O2}, z_{O2}). The O1 and O2 atoms are constrained to have the same occupancy, f_O. In turn, δ, can be calculated as 3(1-f_O). The relative Nd/Ca concentrations have been fixed to the initial quantities used in synthesis. Numbers in parentheses designate the 1σ uncertainty from the refinement.

	$x = 0$		$x = 0.1$		$x = 0.2$		$x = 0.3$		$x = 0.4$	
	9 K	300 K	9 K	300 K	9 K	300 K	9 K	300 K	9 K	300 K
a (Å)	5.3290(1)	5.33480(6)	5.3302(1)	5.3389(1)	5.3303(2)	5.3396(1)	5.3262(2)	5.3387(2)	5.3238(2)	5.3378(2)
b (Å)	7.5410(1)	7.5518(1)	7.5374(2)	7.5502(1)	7.5302(2)	7.5477(2)	7.5203(2)	7.5441(2)	7.5160(2)	7.5420(2)
c (Å)	5.3387(1)	5.3484(1)	5.3353(1)	5.3470(1)	5.3356(2)	5.3474(1)	5.3340(2)	5.3471(2)	5.3259(2)	5.3439(2)
x_{Nd}	0.0363(1)	0.0338(1)	0.0368(2)	0.0336(1)	0.0365(2)	0.0331(2)	0.0356(2)	0.0321(2)	0.0352(3)	0.0317(3)
z_{Nd}	−0.0064(2)	−0.0058(2)	−0.0062(3)	−0.0058(3)	−0.0058(4)	−0.0056(4)	−0.0051(4)	−0.0051(5)	−0.0055(5)	−0.0048(6)
x_{O1}	0.4925(2)	0.4929(2)	0.4913(3)	0.4917(3)	0.4911(4)	0.4913(3)	0.4906(4)	0.4909(4)	0.4904(5)	0.4908(5)
z_{O1}	0.0719(2)	0.0712(3)	0.0717(4)	0.0704(3)	0.0705(4)	0.0688(4)	0.0691(4)	0.0671(5)	0.0680(5)	0.0662(6)
x_{O2}	0.2866(1)	0.2856(2)	0.2870(2)	0.2857(2)	0.2871(3)	0.2862(2)	0.2871(3)	0.2858(3)	0.2874(3)	0.2861(4)
y_{O2}	0.0379(1)	0.0376(1)	0.0377(2)	0.0375(1)	0.0378(2)	0.0376(2)	0.0378(2)	0.0378(2)	0.0374(2)	0.0371(2)
z_{O2}	0.7132(1)	0.7146(2)	0.7134(2)	0.7145(2)	0.7138(3)	0.7147(2)	0.7143(3)	0.7150(3)	0.7133(3)	0.7146(4)
f_O	0.984(3)	0.979(3)	0.956(3)	0.964(3)	0.937(4)	0.948(3)	0.919(4)	0.935(4)	0.927(5)	0.938(5)

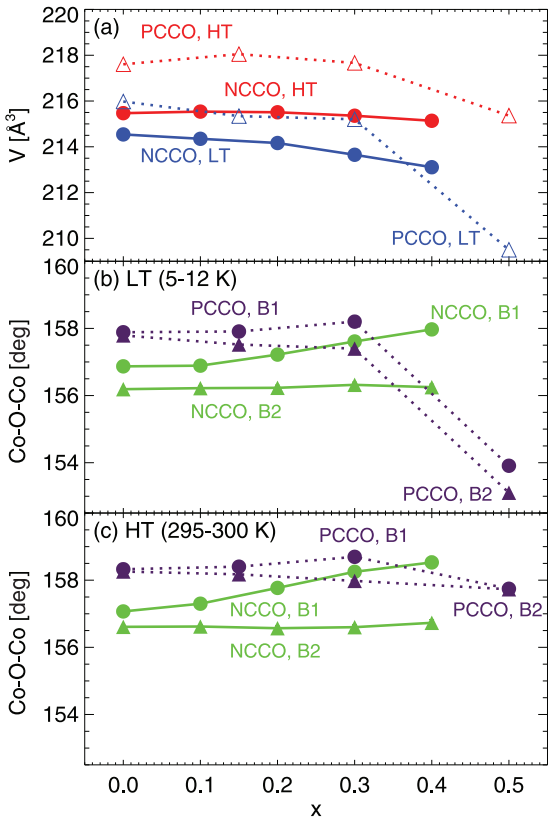

FIG. 2. (Color online) (a) The unit cell volume of NCCO (circles) and PCCO (triangles) as a function of x in two temperature regimes, high temperature (HT) and low temperature (LT). The data for PCCO at $x = 0$ are taken from Ref. 12, $x = 0.15$ and 0.3 come from Ref. 57, and $x = 0.5$ is taken from Ref. 31. The HT data correspond to a temperature of 300 K for the NCCO samples and PCCO $x = 0$, 0.15, and 0.30, and a temperature of 295 K for $x = 0.5$. The LT data correspond to a temperature of 9 K for the NCCO samples, 12 K for PCCO at $x = 0$, 5 K for PCCO at $x = 0.15$, and 0.3, and 10 K for PCCO at $x = 0.5$. (b) The two distinct Co-O-Co bond angles [B1 (circles) and B2 (triangles)] at LT for NCCO (green) and PCCO (purple). (c) The Co-O-Co angles at HT.

angles for $x \leqslant 0.3$, as expected based on the tolerance factor. The only anomaly observed is the reduction in bond angles for $x = 0.5$ PCCO at low temperature, which again arises due to the unique spin-state/metal-insulator transition in that compound.

B. Magnetism

1. dc magnetometry

Figure 3 shows the evolution of zero-field-cooled (ZFC) and field-cooled (FC) magnetization measured in $\mu_o H = 1$ mT as a function of temperature and composition

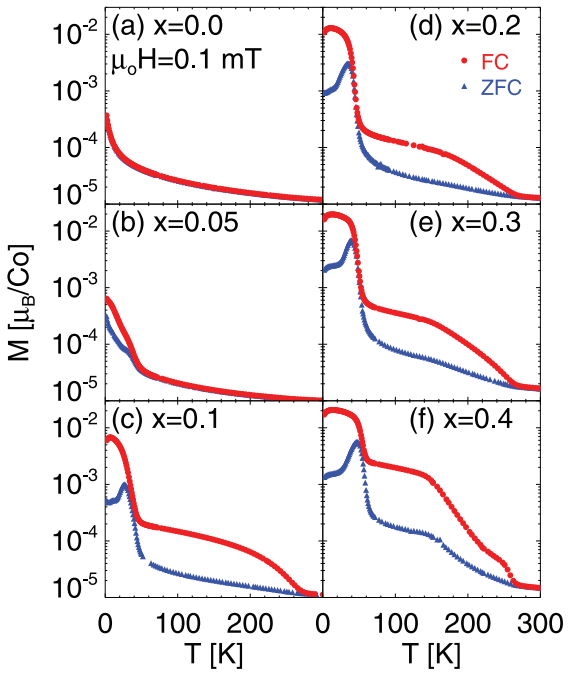

FIG. 3. (Color online) (a)–(f) ZFC and FC magnetization (M) as a function of temperature (in a magnetic field of $\mu_o H = 1$ mT) for multiple x in NCCO. Note that the magnetization axis is on a logarithmic scale.

for NCCO. The parent compound, $x = 0$, is paramagnetic at all measured temperatures, the moment arising from Nd^{3+}. Any contribution from Co^{3+} in this temperature range (i.e., <300 K) is expected to be insignificant, as the ground state of Co^{3+} has $S = 0$ and the spin-state transition to $S = 1$ or $S = 2$ only becomes apparent above approximately 300 K.[15] However, we cannot rule out a contribution to the low-temperature susceptibility from Co arising from surface effects or oxygen deficiency; this is commonly observed as a "Curie tail" in measurements on $LaCoO_3$.[38,39] Although we see no evidence for magnetic ordering at $x = 0$ in these data, the Nd^{3+} moments are known to order antiferromagnetically at $T_N = 1.2$ K, below our lowest measured temperature.[40,41]

Upon increase in x, bifurcation of the ZFC and FC magnetization occurs. This is seen as a rather weak effect for $x = 0.05$ (note that the magnetization is shown here on a logarithmic axis). From $x = 0.10$ to $x = 0.40$ however, several effects become prominent. First, there is a distinct bifurcation between ZFC and FC curves on cooling below about 270 K. This temperature is essentially independent of x, and the effect is nearly identical to that previously observed in PCCO.[18,42] In the PCCO case, SANS measurements directly showed that this bifurcation was due to the formation of SROFM clusters that form a hard magnetic phase. The estimated correlation length was between two and three Co-O-Co distances.[18] Given the measured significant oxygen deficiency in these compounds, the increase in the strength of the high-temperature magnetic contribution with increasing x (where oxygen deficiency becomes increasingly prevalent), and the fact that the magnetic correlation length is as short as two unit cells, we believe that the magnetic polarons and excitons expected to appear around oxygen vacancies[43–45] are a reasonable explanation for the SROFM. Specifically, we refer here to the model of Nagaev and Podel'shchikov,[45] where the high-spin Co^{3+} state is locally stabilized on the Co^{3+} ions near an oxygen vacancy, forming what is referred to as a magnetic exciton. We will discuss this effect again when describing M vs H loops below. The second prominent feature occurs at a much lower temperature, T_C, where both the FC and ZFC magnetizations dramatically increase on cooling, due to the long-range ordering of Co moments (the long-range nature is confirmed by neutron scattering below). As will be returned to a number of times, while this ferromagnetic order is long range, we do not believe that it occupies the entire sample volume, as also found in PCCO.[18] T_C increases with x and reaches a maximum value (as defined by the onset temperature of the increase) of ~60 K for $x = 0.4$. Below T_C, the ZFC and FC magnetizations again bifurcate because the measuring field is significantly smaller than the coercivity (see below). Finally, at a lower temperature (~13 K for $x = 0.4$, for instance), the FC magnetization reaches a maximum and then drops upon further cooling. This effect has not been reported for PCCO[18] but has been observed in $Nd_{1-x}Sr_xCoO_3$, for example,[46,47] suggesting that it is related to the presence of Nd^{3+}. Indeed, neutron diffraction proved that the Nd^{3+} moments order antiparallel to the Co spin sublattice, thereby resulting in a ferrimagnetic structure in $Nd_{1-x}Sr_xCoO_3$.[48] This Nd^{3+} ordering is enhanced by the internal magnetic field generated by the Co sublattice, i.e., by a proximity effect. Thus, we infer that the same ferrimagnetic structure occurs in NCCO. This is also consistent with a nonlinear magnetic field dependence of the crystal field splitting observed in NCCO ($x = 0.3$), which implied that Nd^{3+} moments were oriented either antiparallel or perpendicular to the Co moments.[20] Defining the Nd^{3+} ordering temperature, T_{Ferri}, as the temperature where the maximum FC magnetization occurs, and T_C as the peak in (d^2M/dT^2), we find that the ratio T_{Ferri}/T_C lies between 0.21 and 0.26 (i.e., is approximately constant) for all samples with $x \geqslant 0.075$.

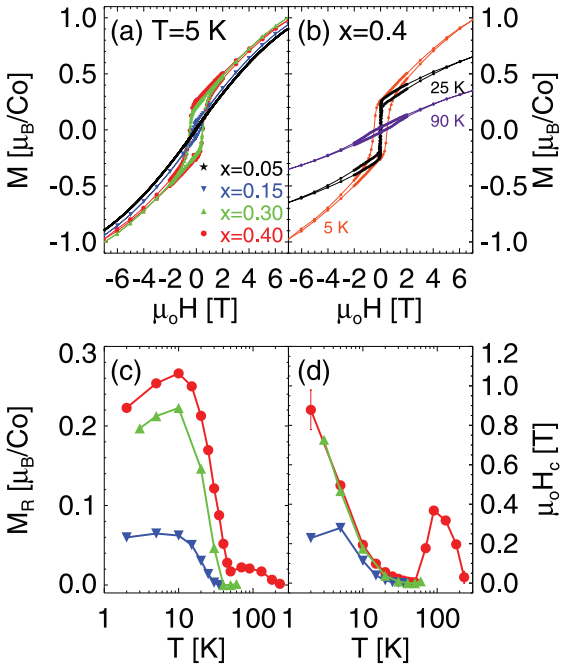

FIG. 4. (Color online) (a) Isothermal magnetization (M) vs magnetic field ($\mu_o H$) hysteresis loops for NCCO $x = 0.05$, 0.15, 0.3, and 0.4 samples at 5 K. (b) M vs H loops for $x = 0.4$ at $T = 5$, 25, and 90 K. (c) Temperature dependence of the remnance (M_R). (d) Temperature dependence of the coercivity ($\mu_o H_c$). The color schemes for panels (c) and (d) are the same as that for (a).

The M vs H loops shown in Figs. 4(a) and 4(b), lend support to the scheme of magnetic transitions described above. As shown in Fig. 4(a) for example, $x = 0.15$, 0.3, and 0.4 samples all have open hysteresis loops at 5 K, consistent with the presence of long-range ferromagnetism. The $x = 0.05$ sample, on the other hand, also has a slightly open loop, but the effect is much weaker than in the higher-doped samples and is not apparent on the scale shown. The coercivity and remnance of the $x = 0.3$ and 0.4 samples are larger than the $x = 0.15$ sample, suggesting a larger ordered moment (or ferromagnetic volume fraction) in the higher-doped samples. The progression of hysteresis loops with decreasing temperature is surprisingly complex, as demonstrated in Fig. 4(b) for $x = 0.4$. At 90 K, which is below the temperature at which the ZFC and FC curves bifurcate (~270 K), but above T_C (~60 K), the loop is indicative of weak but quite hard ferromagnetism—the loop is clearly open and displays large coercivity but with low remnant magnetization. The loops are consistent with this hard phase until the temperature is lowered to T_C and below, at which point the loops assume a "pinched" form [see the 25 K loop, for example, in Fig. 4(b)], where the increasing

field and decreasing field curves are pinched together near $H = 0$ but prominently split at higher fields. This persists to temperatures significantly lower than T_C. As the temperature is further lowered, however, the coercivity increases again, and the pinched form disappears [see the 5-K loop in Fig. 4(b), for instance]. The coercivity [Fig. 4(c)] and remnance [Fig. 4(d)] exemplify the temperature evolution through these three M vs H regimes. On cooling from high temperature, both the coercivity and remnance initially increase below the ZFC/FC bifurcation temperature. They both peak above T_C and then decrease, with the decrease being particularly apparent in the coercivity. After reaching a minimum near T_C, both the remnance and coercivity increase again upon further cooling.

This peculiar progression of M vs H loops was previously documented for PCCO,[18] where it was pointed out that the form of the loops around T_C is, in fact, reminiscent of the exchange-spring behavior commonly observed at hard/soft magnetic interfaces. Indeed, the pinched shape of the hysteresis loops was attributed to exchange-spring-type coupling between the SROFM clusters that appear below the ZFC and FC divergence temperature, which present a high coercivity hysteresis loop, and the LROFM network that begins to form at T_C. The volume fraction of the LROFM phase lying well beneath unity is thus essential for this effect. The qualitatively identical behavior seen here in NCCO leads us to the same conclusion for the origin of this effect. It is, nevertheless, clear that additional work elucidating the exact origins of the oxygen-vacancy-related relatively high-temperature SROFM phase is required.

2. *Magnetic neutron scattering*

The long-range nature of the ferromagnetism below T_C was investigated by magnetic neutron scattering. Figure 5(a) shows the region of the 9-K diffraction patterns around the 001_{pc} reflection (indexed in a pseudocubic setting, where $a \sim 3.8$ Å), with the high-temperature scattering subtracted as a background. This particular reflection has been used to study the ferromagnetic properties of various hole-doped cobaltites[2,9,11,18,49] and is especially useful as its nuclear structure factor is very weak. We observe no peak for $x = 0.0$ and 0.1. However, a peak appears at $x = 0.2$ and becomes more prominent for $x = 0.3$, 0.4. This peak is, in fact, as sharp as the closest nuclear reflection, indicating that it corresponds to long-range magnetic order. The absence of such a peak for $x = 0$ is clearly due to the lack of long-range ferromagnetism, while at $x = 0.1$, we suspect that the ferromagnetic volume fraction is simply too small to be observed in this manner. The integrated intensity of the 001_{pc} peak for $x = 0.4$ is plotted as a function of temperature in Fig. 5(c), where it is seen to have a very similar temperature dependence to the measured squared magnetization, further confirming its magnetic nature. That we are only able to observe a single weak reflection makes magnetic refinement questionable, but we, nevertheless, note that the refined ordered moments at 9 K are 0.39, 0.60, and 0.65 μ_B/Co, with uncertainties of ~0.1 μ_B/Co for the $x = 0.2$, 0.3, and 0.4 samples, respectively. Unsurprisingly, the moment direction could not be uniquely determined. As a final remark on these data, note that the measurements lack the sensitivity required to pick up changes in the Bragg intensity due to the Nd^{3+} ordering, since the ordered Nd^{3+} moment is expected to be much smaller than that of Co, let alone the full Nd^{3+} moment.

We have further studied the magnetic ordering using SANS. As shown in Fig. 5(b), the |Q| dependence of the SANS differential cross section changes as a function of temperature. As the temperature is lowered from 100 to 65 K, there is an increase in scattering for $0.05 < |Q| < 0.2$ Å^{-1}, while little change is observed for $|Q| < 0.05$ Å^{-1}. However, as the temperature is further lowered, there is a significant increase in scattering at $|Q| < 0.03$ Å^{-1}, while the scattering that had appeared in the range $0.05 < Q| < 0.2$ Å^{-1} decreases in intensity. This is better illustrated by the temperature dependence of the intensities at representative values of $|Q| = 0.0079$ Å^{-1} and 0.09 Å^{-1}, as shown in Fig. 5(d). The intensity at $|Q| = 0.0079$ Å^{-1} increases below T_C with a temperature dependence that mimics the magnetization. We attribute this low-$|Q|$ scattering to a Porod term ($I \propto |Q|^{-n}$), arising from the contrast due to ferromagnetic domains with diameter much larger than 100 nm. Fits to a power law yield a temperature-independent n of 4.4. Since $n \approx 4$, this indicates that the scattering comes from three-dimensional objects (magnetic domains in this case) with relatively smooth surfaces. Not only

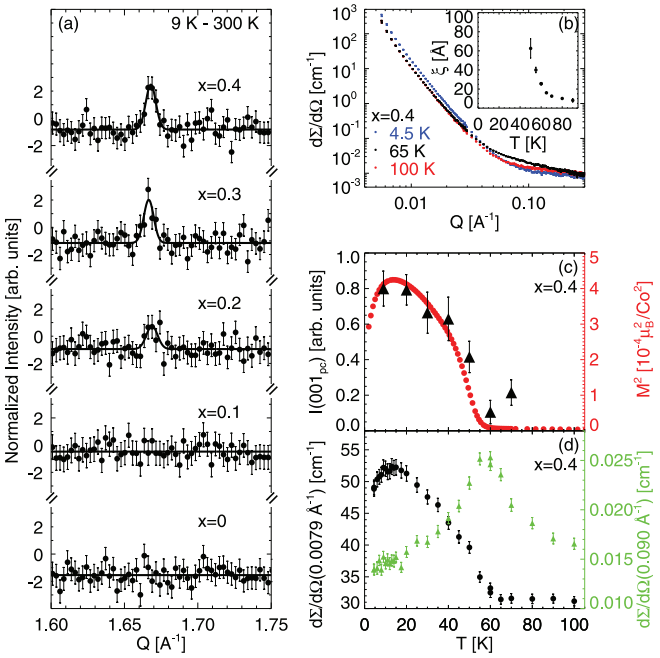

FIG. 5. (Color online) (a) Normalized neutron diffraction intensity in the vicinity of the 001_{pc} peak for NCCO at $x = 0.0, 0.1, 0.2, 0.3,$ and 0.4. The 300-K intensity has been subtracted from the 9-K data as a background. (b) Scattering wave vector ($|Q|$) dependence of the SANS cross section ($d\Sigma/d\Omega$) for $x = 0.4$ at 4.5, 65, and 100 K. The inset shows the estimated correlation length, ξ, as a function of temperature for $x = 0.4$. This was obtained from the inverse of the half-width at half-maximum of a Lorentzian fit to data with $0.032 < |Q| < 0.15$ Å^{-1}, with 120-K data subtracted as a background. (c) Temperature dependence of the integrated intensity of the 001_{pc} peak for $x = 0.4$. The squared magnetization is shown for comparison on the right axis. (d) Temperature dependence of the SANS $d\Sigma/d\Omega$ at $|Q| = 0.0079$ Å^{-1} (left axis) and $|Q| = 0.090$ Å^{-1} (right axis) for $x = 0.4$.

does this low-$|Q|$ scattering increase at T_C, but it also reaches a maximum at the same temperature at which the magnetization does. Hence, the low-$|Q|$ scattering further confirms the reduction in net moment at low temperatures, which we attribute to the antiparallel ordering of the Nd^{3+}sublattice with respect to the Co. The intensity at $|Q| = 0.09$ Å^{-1} has a very different temperature dependence. It increases as the temperature is lowered (above T_C), peaks at T_C, then decreases as the temperature is further lowered. Clearly, this intensity results from short-range ferromagnetic correlations, which are most likely dynamic and diminish at low temperature, where long-range order sets in and the scattering shifts to the Porod component. A simple interpretation is that the peak is a critical scattering peak, which is anticipated for a second-order magnetic phase transition. The divergence as T_C is approached from above corresponds to the appearance of ferromagnetic correlations that have softened into the energy window picked up by SANS, while the divergence as T_C is approached from below arises from the softening of spin-wave excitations. Indeed, we have extracted an estimate for the correlation length as a function of temperature [inset to Fig 5(b)], which diverges as the temperature is cooled through T_C as expected. The fact that this high-$|Q|$ scattering component does not completely disappear as $T \rightarrow 0$, as in PCCO,[18] is again consistent with a LROFM volume fraction below unity, even in the low T limit. One may ask why no critical scattering is observed at the ferrimagnetic transition. The absence of the critical scattering in this case is due to the Nd^{3+} moments ordering within the presence of the large internal magnetic field from the Co sublattice. Essentially, the Zeeman splitting in this large exchange field suppresses the fluctuations that give rise to a critical scattering peak.

3. *ac magnetometry*

We have further studied the magnetic ordering using ac magnetometry. Figure 6 shows the real (χ') and imaginary (χ'') parts of the magnetic susceptibility for $x = 0.1$, 0.15, and 0.3. The main feature for all three samples is that both χ' and χ'' exhibit a maximum near T_C. Since χ diverges at a conventional second-order ferromagnetic phase transition, this is expected. However, the frequency dependence allows us to observe whether there are slow dynamics on a laboratory timescale. Although we have already established that there are ferromagnetic correlations in these samples, a frequency-dependent freezing temperature could be indicative of a cluster glasslike state, or at least an unusually glassy magnetic response. Indeed, studies of LSCO have noted significant frequency dependence in both the spin-glass and ferromagnetic regions of the LSCO phase-diagram.[50–52] Glassy behavior has also been observed through aging effects in LSCO.[53]

For NCCO, we do indeed observe a noticeable frequency dependence to the freezing temperature for all three samples, with the magnitude of the peak in χ' becoming weaker, and the freezing temperature itself becoming larger, as the frequency is increased. If we define $\Delta T_f = T_f$ (1000 Hz) $- T_f$ (1.7 Hz), then we obtain $\Delta T_f = 1.09$ K, 0.95 K, and 0.62 K for $x = 0.1$, 0.15, and 0.3, respectively. As a means of comparison, we estimate that based on the fitting parameters in Ref. 50, polycrystalline LSCO with $x = 0.09$ has $\Delta T_f = 1.12$ K (over the same frequency range), very similar to NCCO with $x = 0.1$. Clearly, the fact that long-range ferromagnetic correlations develop in these NCCO samples indicates that force fitting to a Vogel-Fulcher law or to the critical slowing down of spin dynamics for a spin glass is inappropriate. What these data do tell us, however, is that there is indeed glassiness to the magnetic ordering behavior, and that this glassiness becomes weaker as x is increased, since ΔT_f decreases. Such behavior is consistent with that seen in several perovskite cobaltite systems and can be understood in terms of a crossover (not necessarily complete) from magnetic phase separation at low doping to a uniform ferromagnetic metallic state at higher doping.

C. Transport

The resistivity, ρ, of NCCO is shown as a function of temperature and x in Fig. 7(a). As with all other hole-doped perovskite cobaltites, ρ decreases as x is increased. In fact, the resistivity decreases quite rapidly with x, significantly faster than in LSCO, for instance,[50] an unexpected feature. For all samples measured, we find $d\rho/dT < 0$ as $T \rightarrow 0$. While this condition is often used as an approximate criterion for classifying a ground state as an insulator, a more rigorous criterion to distinguish metallic and insulating states hinges on whether the conductivity, σ, extrapolates to a finite value as $T \rightarrow 0$. The temperature dependence of σ is thus displayed in Fig. 7(b) for all the samples shown in Fig. 7(a). While the base temperature of our study is relatively high (4.2 K), it is clear that a large increase in low-temperature conductivity occurs between 0.1 and 0.2, which we believe likely marks the IMT. Further studies with single-crystal samples will be required to refine this conclusion as the true T dependence of the conductivity is no doubt somewhat masked by grain boundary effects.

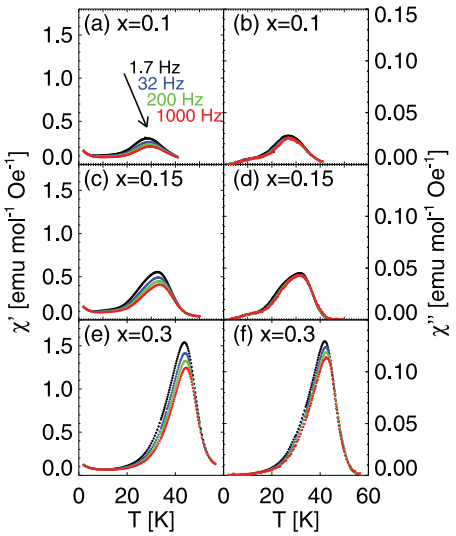

FIG. 6. (Color online) Temperature dependence of the real (χ', left panels) and imaginary (χ'', right panels) components of the ac magnetic susceptibility for NCCO at $x = 0.1$, 0.15, and 0.30. Measurements were performed with an ac field amplitude of $\mu_o H = 0.4$ mT.

The onset of LROFM is also apparent in the transport. As an example, Fig. 7(b) shows that the $x = 0.4$ sample clearly shows an enhancement in σ around T_C. This effect is shown more clearly in Fig. 8(a) and its inset, which shows the resistivity of the $x = 0.3$ sample under $\mu_o H = 0$T and $\mu_o H = 9$ T. The two curves separate such that the $\mu_o H = 9$ T resistivity is measurably lower over a broad temperature range from about 10 to 200 K. This is more clearly displayed in Fig. 8(b), which shows the magnetoresistance, defined as $\mathrm{MR} = 100\% \times [\rho(\mu_o H) - \rho(0T)]/\rho(0T)$, at $\mu_o H = 9$ T. A negative peak in the MR at T_C has been reported in the ferromagnetic regime of LSCO,[8,50] where it results from field-induced suppression in spin-disorder scattering. For the present case of NCCO ($x = 0.3$), the conductivity is clearly "less metallic" in the sense that the absolute conductivity values are lower and $d\rho/dT$ remains negative, as noted above. The narrow electronic bandwidth in systems such as NCCO and PCCO apparently results in transport rather close to the metal-insulator boundary, even at substantial doping. The resultant weakly diffusive transport at compositions such as $x = 0.3$, likely occurring only through a marginally percolated ferromagnetic network, is no doubt responsible for the significantly reduced MR peak in $\mu_0 H = 9$ T in NCCO (~3%) compared to the wider bandwidth LSCO (~7%).[50] Figures 8(c)–8(e) show field sweeps of the MR above T_C (90 K), near T_C (50 K), and below T_C (30 K), respectively. The main feature seen in these sweeps is that the shape transforms from "rounded" above T_C to "cusplike" at T_C and below, a common feature of colossal magnetoresistive (CMR)-type materials.[26,50] Because the negative MR typically scales with the square of the magnetization, i.e., $\mathrm{MR} \propto (M/M_s)^2$, these different shapes simply reflect the difference in the field dependence of the magnetization above and below T_C,[26] which controls the spin-disorder contribution to the resistivity.

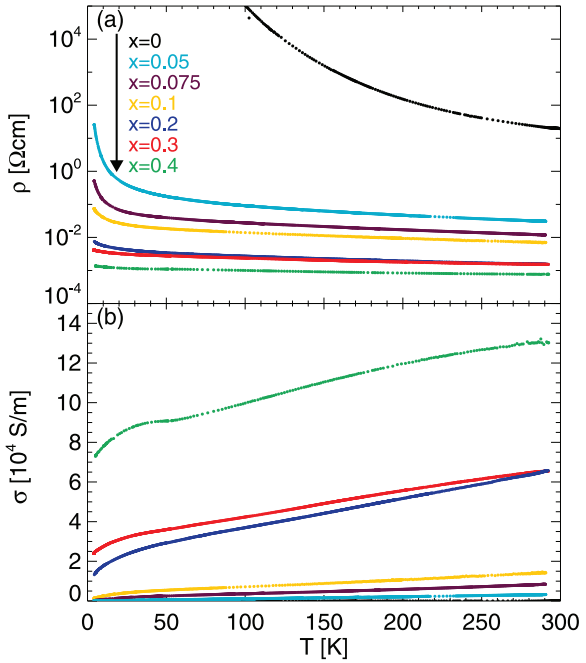

FIG. 7. (Color online) Temperature dependence of (a) the resistivity (ρ) and (b) the conductivity (σ) for NCCO at $x = 0.0$, 0.05, 0.075, 0.1, 0.2, 0.3, and 0.4.

IV. DISCUSSION AND CONCLUSIONS

By combining the magnetometry, magnetic neutron scattering, and transport data presented above, a phase diagram was established, as shown in Fig. 9. Samples with $x \geqslant 0.1$ are paramagnetic at high temperatures, then enter a regime of SROFM of the Co moments below ~270 K. LROFM of Co moments sets in only at a much lower temperature, and finally the Nd^{3+} moments order at an even lower temperature. For samples with $x < 0.1$, identification of the phases is less clear. There is still some splitting between the ZFC and FC magnetization around 270 K, but with significantly reduced magnitude compared to samples with $x \geqslant 0.1$. For samples with $x \geqslant 0.075$, we are able to identify a T_C and a T_{Ferri}; however, as illustrated for the $x = 0.05$ sample in Fig. 3(b), while there is certainly some low-temperature splitting between the ZFC and FC magnetization, suggesting some type of freezing, the effect is so weak that it is not clearly appropriate to label the ground state as ferromagnetic. Note that it is only the log scale on the magnetization axis that allows this weak effect to be discernible in such plots. From Fig. 4(a), it is apparent that the 5 K M vs H loop is less open than for higher x samples. Nevertheless, the sample is clearly not a simple paramagnet and obviously exhibits ferromagnetic correlations. For this reason, we have shaded the phase diagram with a color gradient from $x = 0$ to $x = 0.075$ to reflect the ambiguity in the nature of the magnetic states. As discussed

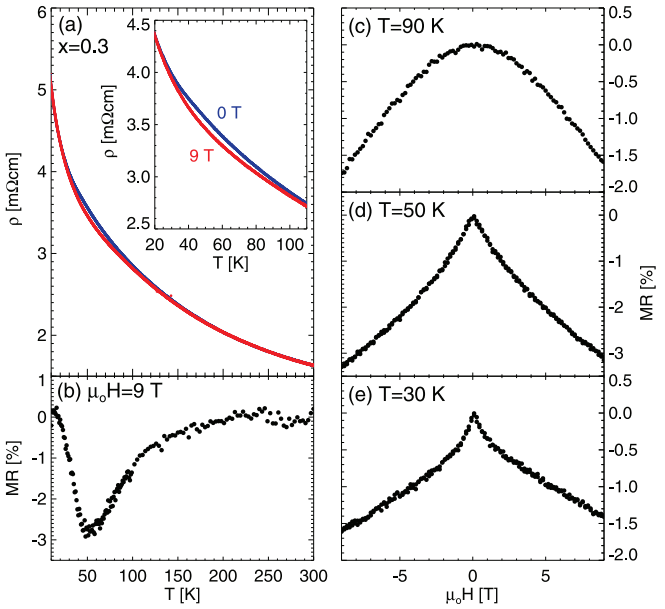

FIG. 8. (Color online) (a) The temperature dependence of the resistivity (ρ) in magnetic fields of $\mu_o H = 0$ T and $\mu_o H = 9$ T for $Nd_{0.7}Ca_{0.3}CoO_{3-\delta}$. The same data are shown in the inset over a narrower temperature range around the Curie point. (b) MR extracted from the data in panel (a). The definition of MR is given in the text. (c)–(e) Isothermal field sweeps of the MR at 90, 50, and 30 K, respectively. The applied magnetic field is perpendicular to the current (and thus the sample plane) for all measurements shown.

above, there is a large increase in the conductivity between $x = 0.1$ and $x = 0.2$, which we believe likely marks the IMT. We have thus indicated the IMT at a point between $x = 0.1$ and $x = 0.2$, although additional work on single crystals will be required to further pin this down.

A major impetus for the present study was to use the NCCO system as a point of comparison for the PCCO system, for which the unique IMT and spin-state transition has been attributed to a Pr-valence transition. It is thus of high interest to directly compare the phase diagrams of PCCO and NCCO. The scattering data for NCCO and PCCO indicate that, at least for $x \leqslant 0.3$, the structures of these two materials are very similar, with the main difference being that the Co-O-Co bond angles are slightly more buckled in the NCCO series. Due to this difference in bond angles, we would naively expect that the main difference between PCCO and NCCO would be that NCCO would have a marginally lower T_C. Any other differences should be a manifestation of physics coming from the rare-earth site. The phase diagram of PCCO was shown in Ref. 18. The two phase diagrams are similar in the sense that SROFM is observed around the same temperature in both systems and that a ferromagnetic metallic state develops with doping. Moreover, the maximum T_C observed in PCCO is ~70 K, compared to ~60 K for NCCO, which is reasonable considering the Co-O-Co bond angles. However, the PCCO phase diagram shows a transition to the ferromagnetic metallic state at a much higher doping, with the sample in a paramagnetic insulating state for $x \leqslant 0.2$, distinctly different than NCCO, where ferromagnetism is already apparent at $x = 0.075$. We believe that this difference can be largely attributed to oxygen content. These narrow bandwidth cobaltites have final oxygen contents that are quite sensitive to preparation conditions.[32] In particular, the NCCO samples measured in the present study were annealed and slow cooled in flowing O_2 gas, whereas the PCCO samples in Ref. 18 were prepared under slightly different conditions and from a different Co source material. We speculate that this led to higher oxygen deficiency in PCCO in Ref. 18 than in the current work on NCCO. We have confirmed that this is the case by synthesizing the mixed compound $(Nd_{1-y}Pr_y)_{0.85}Ca_{0.15}CoO_3$ by annealing and slow cooling in flowing O_2 gas (i.e., the same preparation conditions as used here for NCCO). We found ferromagnetic ordering across the entire range of y, confirming that both PCCO and NCCO similarly enter the ferromagnetic metallic state at relatively low doping, certainly by $x = 0.15$. (The reasons for entry into the ferromagnetic regime at such low x values compared to higher bandwidth systems such as LSCO remains unclear.) Hence, there are only two main differences between NCCO and PCCO. The first is that Nd^{3+} ions order antiparallel to the Co sublattice, forming a ferrimagnetic ground state, while the Pr^{3+} ions do not order at all. The reason for this difference lies in the crystalline electric field levels of these two ions. Specifically, Pr^{3+} ions have a singlet ground state,[54] which prevents ordering in the absence of a strong exchange interaction,[55] while Nd^{3+} ions have a Kramer's doublet ground state[54] that can order. This is also the reason why an antiferromagnetic ground state is observed in undoped $NdCoO_3$ but not in undoped $PrCoO_3$. The second difference is the Pr valence transition that occurs in $x = 0.5$ PCCO samples. In the composition range studied here in NCCO, we see no such effect and indeed no structural precursor of the onset of such an effect at higher x (e.g., Fig. 2). This conclusion comes with the caveat that we are unable to synthesize phase-pure $x = 0.5$ NCCO and thus cannot rule out a possible valence transition at that composition. Note however that previous studies of Y-doped NCCO ($x = 0.3$) also revealed no evidence for valence transitions, whereas Y-doped PCCO ($x = 0.3$) does exhibit such a valence transition.[31] This also supports our suggestion that there is no Nd valence transition. Furthermore, first-principles calculations indicate that the Nd $4f$ occupied states lie too far below the Fermi level for there to be such a Nd valence transition in NCCO, in contrast to the situation with Pr in PCCO.[21]

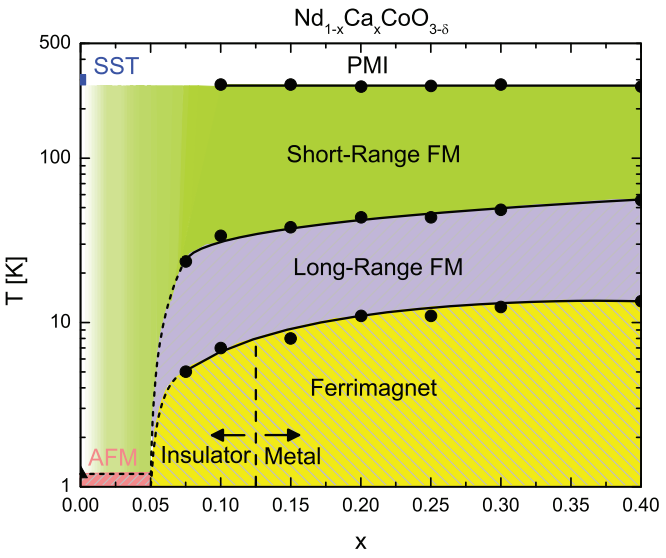

FIG. 9. (Color online) Magnetic and electronic phase diagram of NCCO. Note that the temperature axis is on a log scale. The values for the onset of short-range-ordered ferromagnetism were determined from the splitting of the ZFC-FC magnetization in a magnetic field of $\mu_o H = 1$ mT. The values of the Curie temperature, T_C, were determined from the peak in (d^2M/dT^2) in $\mu_o H = 1$ mT. The values of T_{Ferri} were determined from the maximum in the FC magnetization in $\mu_o H = 1$ mT. The spin-state transition temperature (SST) comes from Ref. 15. The Néel temperature, T_N, for the parent compound comes from Refs. 40,41. The color fading from $x = 0$ to 0.05 is meant to indicate uncertainty in the magnetic phase over that composition range, as described in the text. The IMT occurs between $x = 0.1$ and 0.2, and the exact placement at $x = 0.125$ is arbitrary.

As noted above, both PCCO and NCCO exhibit a splitting between ZFC and FC susceptibility at relatively high temperatures (~270 K for NCCO), attributed to SROFM. It is suspected that this magnetism is related to oxygen deficiency, as we have observed that the magnitude of this feature depends quite strongly on annealing conditions in PCCO[56] and becomes more prominent as x is increased and the samples become more difficult to fully oxygenate. The ordering temperature does not seem to depend on the oxygen deficiency concentration or on x. We are unable to detect the magnetic cross section from this phase in our SANS experiments. A point of future work would be to perform neutron diffraction measurements on single crystals to more clearly elucidate the precise nature of this phase. Below T_C,

there is a coupling between this SROFM phase and the LROFM phase, resulting in the exchange-spring behavior apparent in both PCCO and NCCO, indicating that there are at least two coexisting magnetic states. Coexisting phases are possible because the volume fraction of LROFM is significantly smaller than unity. This is evidenced by the small ordered moment observed by neutron diffraction in NCCO and PCCO (e.g., 0.6 μ_B/Co for NCCO compared to ~1.7 μ_B/Co for LSCO[11] at $x = 0.3$), the lack of complete long-range static ferromagnetic order from SANS at low T,[18] and the nature of the transport and magnetotransport. The nature of the interfacial coupling between the SROFM and LROFM phases remains poorly understood and will hopefully be the focus of future work.

In summary, we have studied the structure of NCCO by neutron diffraction and found that the structure is orthorhombic between 10 and 300 K for $x \leqslant 0.4$ and is indeed very similar to that reported for PCCO. We investigated the magnetic properties by neutron diffraction, SANS, dc magnetometry, and ac magnetometry. SROFM appears below ~270 K, likely related to oxygen deficiency, while LROFM sets in at a much lower temperature (maximum $T_C \sim 60$ K), which can be qualitatively understood in terms of the reduced bandwidth. Around T_C, the hysteresis loops clearly indicate exchange-spring behavior (as in PCCO) arising from the coexistence of the hard SROFM phase and the soft LROFM phase. At $T_{\text{Ferri}} \sim 0.25\ T_C$, the Nd^{3+}sublattice orders antiparallel to the Co sublattice. Transport measurements show that the conductivity dramatically increases upon hole substitution, with an IMT likely occurring between $x = 0.1$ and 0.2. The LROFM is evident as both an anomaly in the temperature dependence of the conductivity as well as a negative peak in the MR. These results have been summarized on a magnetic phase diagram. Although much of this behavior can be at least qualitatively understood, one surprising feature, yet to be rationalized, is that LROFM, while suppressed to substantially lower T_C, actually turns on at *lower x* than in higher bandwidth cobaltites. Further work will be required to understand this.

ACKNOWLEDGMENTS

This work was supported primarily by the Basic Energy Sciences, US Department of Energy (DOE) under Grant No. DE-FG02-06ER46275. We gratefully acknowledge fruitful discussions with Shameek Bose and Stephan Rosenkranz, experimental assistance on NG-3 from Steve Kline, and experimental assistance on POWGEN from Luke Heroux. Research conducted at Oak Ridge National Laboratory's Spallation Neutron Source was sponsored by the Scientific User Facilities Division, Office of Basic Energy Sciences, US DOE. This work was carried out in part using computing resources at the University of Minnesota Supercomputing Institute. This work used facilities at NIST supported in part by the National Science Foundation under DMR-0944772.

[1] A. Podlesnyak, S. Streule, J. Mesot, M. Medarde, E. Pomjakushina, K. Conder, A. Tanaka, M. W. Haverkort, and D. I. Khomskii, Phys. Rev. Lett. **97**, 247208 (2006).

[2] D. Phelan, D. Louca, S. Rosenkranz, S.-H. Lee, Y. Qiu, P. J. Chupas, R. Osborn, H. Zheng, J. F. Mitchell, J. R. D. Copley, J. L. Sarrao, and Y. Moritomo, Phys. Rev. Lett. **96**, 027201 (2006).

[3] M. A. Korotin, S. Y. Ezhov, I. V. Solovyev, V. I. Anisimov, D. I. Khomskii, and G. A. Sawatzky, Phys. Rev. B **54**, 5309 (1996).

[4] M. W. Haverkort, Z. Hu, J. C. Cezar, T. Burnus, H. Hartmann, M. Reuther, C. Zobel, T. Lorenz, A. Tanaka, N. B. Brookes, H. H. Hsieh, H.-J. Lin, C. T. Chen, and L. H. Tjeng, Phys. Rev. Lett. **97**, 176405 (2006).

[5] S. Yamaguchi, Y. Okimoto, H. Taniguchi, and Y. Tokura, Phys. Rev. B **53**, R2926 (1996).

[6] A. Podlesnyak, M. Russina, A. Furrer, A. Alfonsov, E. Vavilova, V. Kataev, B. Büchner, T. Strässle, E. Pomjakushina, K. Conder, and D. I. Khomskii, Phys. Rev. Lett. **101**, 247603 (2008).

[7] C. He, S. El-Khatib, J. Wu, J. W. Lynn, H. Zheng, J. F. Mitchell, and C. Leighton, Europhys. Lett. **87**, 27006 (2009).

[8] J. Wu, J. W. Lynn, C. J. Glinka, J. Burley, H. Zheng, J. F. Mitchell, and C. Leighton, Phys. Rev. Lett. **94**, 037201 (2005).

[9] D. Phelan, D. Louca, K. Kamazawa, S.-H. Lee, S. N. Ancona, S. Rosenkranz, Y. Motome, M. F. Hundley, J. F. Mitchell, and Y. Moritomo, Phys. Rev. Lett. **97**, 235501 (2006).

[10] A. M. Glazer, Acta Crystallogr. Sec. B **28**, 3384 (1972).

[11] R. Caciuffo, D. Rinaldi, G. Barucca, J. Mira, J. Rivas, M. A. Senaris-Rodriguez, P. G. Radaelli, D. Fiorani, and J. B. Goodenough, Phys. Rev. B **59**, 1068 (1999).

[12] J. Yu, D. Phelan, and D. Louca, Phys. Rev. B **84**, 132410 (2011).

[13] K. Knížek, J. Hejtmánek, Z. Jirák, P. Tomeš, P. Henry, and G. André, Phys. Rev. B **79**, 134103 (2009).

[14] Y. Ren, J.-Q. Yan, J.-S. Zhou, J. B. Goodenough, J. D. Jorgensen, S. Short, H. Kim, T. Proffen, S. Chang, and R. J. McQueeney, Phys. Rev. B **84**, 214409 (2011).

[15] J.-Q. Yan, J.-S. Zhou, and J. B. Goodenough, Phys. Rev. B **69**, 134409 (2004).

[16] M. Tachibana, T. Yoshida, H. Kawaji, T. Atake, and E. Takayama-Muromachi, Phys. Rev. B **77**, 094402 (2008).

[17] A. O. Sboychakov, K. I. Kugel, A. L. Rakhmanov, and D. I. Khomskii, Phys. Rev. B **80**, 024423 (2009).

[18] S. El-Khatib, S. Bose, C. He, J. Kuplic, M. Laver, J. A. Borchers, Q. Huang, J. W. Lynn, J. F. Mitchell, and C. Leighton, Phys. Rev. B **82**, 100411 (2010).

[19] S. Tsubouchi, T. Kyômen, M. Itoh, P. Ganguly, M. Oguni, Y. Shimojo, Y. Morii, and Y. Ishii, Phys. Rev. B **66**, 052418 (2002).

[20] J. Hejtmánek, E. Šantavá, K. Knížek, M. Maryško, Z. Jirák, T. Naito, H. Sasaki, and H. Fujishiro, Phys. Rev. B **82**, 165107 (2010).

[21] K. Knížek, J. Hejtmánek, P. Novák, and Z. Jirák, Phys. Rev. B **81**, 155113 (2010).

[22] A. J. Barón-González, C. Frontera, J. L. García-Muñoz, J. Blasco, and C. Ritter, Phys. Rev. B **81**, 054427 (2010).

[23] J. L. García-Muñoz, C. Frontera, A. J. Barón-González, S. Valencia, J. Blasco, R. Feyerherm, E. Dudzik, R. Abrudan, and F. Radu, Phys. Rev. B **84**, 045104 (2011).

[24]C. Leighton, D. D. Stauffer, Q. Huang, Y. Ren, S. El-Khatib, M. A. Torija, J. Wu, J. W. Lynn, L. Wang, N. A. Frey, H. Srikanth, J. E. Davies, K. Liu, and J. F. Mitchell, Phys. Rev. B **79**, 214420 (2009).
[25]M. E. López-Morales, D. Ríos-Jara, J. Tagüena, R. Escudero, S. LaPlaca, A. Bezinge, V. Y. Lee, E. M. Engler, and P. M. Grant, Phys. Rev. B **41**, 6655 (1990).
[26]J. M. D. Coey, M. Viret, and S. von Molnár, Adv. Phys. **48**, 167 (1999).
[27]A. C. Larson and R. B. Von Dreele, General Structure Analysis System (GSAS), Los Alamos National Laboratory Report LAUR 86-748 (2004).
[28]B. H. Toby, J. Appl. Crystallogr. **34**, 210 (2001).
[29]C. J. Glinka, J. G. Barker, B. Hammouda, and S. Krueger, J. Appl. Crystallogr. **31**, 430 (1998).
[30]S. R. Kline, J. Appl. Crystallogr. **39**, 895 (2006).
[31]T. Fujita, T. Miyashita, Y. Yasui, Y. Kobayashi, M. Sato, E. Nishibori, M. Sakata, Y. Shimojo, N. Igawa, Y. Ishii, K. Kakurai, T. Adachi, Y. Ohishi, and M. Takata, J. Phys. Soc. Jpn. **73**, 1987 (2004).
[32]P. Tong, Y. Wu, B. Kim, D. Kwon, J. M. S. Park, and B. G. Kim, J. Phys. Soc. Jpn. **78**, 034702 (2009).
[33]C. N. R. Rao, J. Gopalakrishnan, and K. Vidyasagar, Indian J. Chem., Sec. A. **23**, 265 (1984).
[34]V. P. Kumar, Y. S. Reddy, P. Kistaiah, and C. V. Reddy, Mater. Res. Innovations **14**, 68 (2010).
[35]S. Kolesnik, B. Dabrowski, J. Mais, M. Majjiga, O. Chmaissem, A. Baszczuk, and J. D. Jorgensen, Phys. Rev. B **73**, 214440 (2006).
[36]R. D. Shannon, Acta Crystallogr. Sec. A **32**, 751 (1976).
[37]T. Kimura and Y. Tokura, in *High Magnetic Fields: Applications in Condensed Matter Physics and Spectroscopy*, edited by C. Berthier, L. P. Lévy, and G. Martinez (Springer-Verlag, Berlin, 2001), pp. 364–365.
[38]S. R. Giblin, I. Terry, D. Prabhakaran, A. T. Boothroyd, and C. Leighton, Phys. Rev. B **79**, 174410 (2009).
[39]J.-Q. Yan, J.-S. Zhou, and J. B. Goodenough, Phys. Rev. B **70**, 014402 (2004).
[40]F. Bartolomé, M. D. Kuz'min, J. Bartolomé, J. Blasco, J. García, and F. Sapiña, Solid State Commun. **91**, 177 (1994).
[41]I. Plaza, E. Palacios, J. Bartolomé, S. Rosenkranz, C. Ritter, and A. Furrer, Physica B **234-236**, 632 (1997).
[42]M. Maryško, Z. Jirák, J. Hejtmánek, and K. Knížek, J. Appl. Phys. **111**, 07E110 (2012).
[43]S. R. Giblin, I. Terry, D. Prabhakaran, A. T. Boothroyd, J. Wu, and C. Leighton, Phys. Rev. B **74**, 104411 (2006).
[44]S. R. Giblin, I. Terry, S. J. Clark, T. Prokscha, D. Prabhakaran, A. T. Boothroyd, J. Wu, and C. Leighton, Europhys. Lett. **70**, 677 (2005).
[45]E. L. Nagaev and A. I. Podel'shchikov, J. Phys.: Condens. Matter **8**, 5611 (1996).
[46]M. Paraskevopoulos, J. Hemberger, A. Krimmel, and A. Loidl, Phys. Rev. B **63**, 224416 (2001).
[47]D. D. Stauffer and C. Leighton, Phys. Rev. B **70**, 214414 (2004).
[48]A. Krimmel, M. Reehuis, M. Paraskevopoulos, J. Hemberger, and A. Loidl, Phys. Rev. B **64**, 224404 (2001).
[49]J. Yu, D. Louca, D. Phelan, K. Tomiyasu, K. Horigane, and K. Yamada, Phys. Rev. B **80**, 052402 (2009).
[50]J. Wu and C. Leighton, Phys. Rev. B **67**, 174408 (2003).
[51]D. N. H. Nam, K. Jonason, P. Nordblad, N. V. Khiem, and N. X. Phuc, Phys. Rev. B **59**, 4189 (1999).
[52]D. Samal and P. S. Anil Kumar, J. Phys.: Condens. Matter **23**, 016001 (2011).
[53]M. Itoh, I. Natori, S. Kubota, and K. Motoya, J. Phys. Soc. Jpn. **63**, 1486 (1994).
[54]S. Rosenkranz, M. Medarde, F. Fauth, J. Mesot, M. Zolliker, A. Furrer, U. Staub, P. Lacorre, R. Osborn, R. S. Eccleston, and V. Trounov, Phys. Rev. B **60**, 14857 (1999).
[55]Y. L. Wang and B. R. Cooper, Phys. Rev. **172**, 539 (1968).
[56]K. Bhatti, M. Taylor, S. Bose, and C. Leighton (unpublished).
[57]S. El Khatib and C. Leighton, (private communication).